

# JAAS

Accepted Manuscript



This is an *Accepted Manuscript*, which has been through the Royal Society of Chemistry peer review process and has been accepted for publication.

*Accepted Manuscripts* are published online shortly after acceptance, before technical editing, formatting and proof reading. Using this free service, authors can make their results available to the community, in citable form, before we publish the edited article. We will replace this *Accepted Manuscript* with the edited and formatted *Advance Article* as soon as it is available.

You can find more information about *Accepted Manuscripts* in the [Information for Authors](#).

Please note that technical editing may introduce minor changes to the text and/or graphics, which may alter content. The journal's standard [Terms & Conditions](#) and the [Ethical guidelines](#) still apply. In no event shall the Royal Society of Chemistry be held responsible for any errors or omissions in this *Accepted Manuscript* or any consequences arising from the use of any information it contains.

## Laser ablation low-flow ICP-MS for elemental bioimaging

Tobias Steingrobe<sup>a,†</sup>, Ann-Christin Niehoff<sup>a,b,†</sup>, Bastian Franze<sup>a</sup>, Diana Lenhard<sup>d</sup>, Hubertus Pietsch<sup>c</sup>,  
Carsten Engelhard<sup>e</sup>, Uwe Karst<sup>a</sup>, Wolfgang Buscher<sup>a</sup>

a University of Münster, Institute of Inorganic and Analytical Chemistry, Corrensstr. 30, 48149 Münster  
Germany.

b NRW Graduate School of Chemistry, University of Münster, Germany

c Bayer Pharma AG, MR and CT Contrast Media Research, Müllerstr 178, 13353 Berlin, Germany.

d Charité-Universitätsmedizin, Institute for Vegetative Physiology, Hessische Str. 3-4, 10115 Berlin,  
Germany

e University of Siegen, Department of Chemistry & Biology, Adolf-Reichwein-Str. 2, 57076 Siegen,  
Germany.

† The authors contributed equally to this work.

### Abstract

A laser ablation system (LA) was coupled to an in-house developed low-flow inductively coupled plasma ion source for mass spectrometry (ICP-MS). In this set-up, the low-flow torch showed best analytical performance at a total argon gas flow rate of only 1.27 L/min and a generator power of 900 W. The optimized system was applied to elemental bioimaging. Two different sections of one kidney sample were analyzed and images of the elements Al and Br from the staining agents hematoxylin and eosin, respectively, and I from contrast agent iodixanol were recorded selectively and with high sensitivity. For detection of the elements, the mass traces <sup>27</sup>Al, <sup>79</sup>Br, <sup>81</sup>Br, and <sup>127</sup>I were selected to demonstrate the system's analytical performance over a wide mass range. In total, the argon consumption could be reduced by > 90% compared to conventional ICP-MS systems.

25

**26 Introduction**

27 The analysis of the elemental distribution in biological samples has gained increasing research interests  
28 in recent years. Various biochemical species of elements have been identified as important components  
29 in organisms exhibiting beneficial or detrimental effects. Bioimaging of elemental distributions has  
30 therefore significantly gained importance and scientific recognition.<sup>1-5</sup> One of the most popular  
31 techniques in elemental bioimaging is the hyphenation of laser ablation with inductively coupled plasma  
32 mass spectrometry (LA-ICP-MS). This technique combines the high spatial resolution of laser ablation in  
33 the micrometer range with a highly sensitive, element selective detector system.<sup>6-8</sup> One of the major  
34 drawbacks of this technique is the high argon gas consumption of approximately 15-20 L/min. To  
35 generate well resolved images of organs and organ sections with LA-ICP-MS, small laser spot sizes and a  
36 fairly slow sample movement are necessary. Consequently, the measurement of an image takes several  
37 hours. This may result in a total argon consumption of several thousand liters of argon per bioimage.

38 Since the introduction of the ICP, several approaches were investigated to reduce the Ar consumption.  
39 To avoid the high cooling gas flows that constitute the largest portion of the ICP's gas consumption,  
40 alternative cooling strategies for the quartz torch were investigated. Most approaches dealt with water-  
41 cooling<sup>9-13</sup>, air-cooling<sup>13-15</sup> and miniaturization<sup>16, 17</sup> of the ICP torch. Some work was focused on radiative  
42 cooling by means of ceramic materials, like Al<sub>2</sub>O<sub>3</sub> and BN.<sup>18, 19</sup>

43 A torch for ICP coupled with optical emission spectrometry (ICP-OES) with only 1 L/min Ar consumption  
44 compared to Fassel-type torches was first presented by Klostermeier et al..<sup>20</sup> The authors called this new  
45 approach Static High sensitivity ICP (SHIP). As cooling medium, compressed air was used, thus allowing  
46 the complete removal of the conventional ICP's cooling argon gas flow. The torch geometry was changed  
47 significantly compared to Fassel-type torches: The main part of the quartz torch was bubble shaped and

1  
2  
3 48 contained a plasma that was formed like a sphere inside the load coil area of the ICP. It fit exactly into  
4  
5 49 the load coil of a commercial ICP-OES spectrometer.  
6  
7

8  
9 50 Scheffer et al. carried out first successful experiments to transfer this approach to an ICP-MS  
10  
11 51 spectrometer. They still reported secondary discharges and polyatomic interferences which were caused  
12  
13 52 by the interaction of plasma and the stream of cooling air.<sup>21</sup> In 2012, Pfeifer et al. presented an  
14  
15 53 optimized version of this type of low-flow torch.<sup>22</sup> They developed a new sampling interface to minimize  
16  
17 54 the interaction of plasma and cooling air stream. The removal of the secondary discharge was achieved  
18  
19 55 by use of an electrostatic platinum shield. The limits of detection were found to be only slightly inferior  
20  
21 56 compared to the conventional ICP-MS. However, the background of the low-flow torch was significantly  
22  
23 57 lower than achieved with conventional torches. The authors could demonstrate the capability of the new  
24  
25 58 low-flow ICP-MS in speciation analysis by its hyphenation with gas chromatography (GC) and high  
26  
27 59 performance liquid chromatography (HPLC).  
28  
29  
30  
31

32 60 The torch presented here is based on these developments, but was further optimized with respect to the  
33  
34 61 gas connectors and gas flow capillaries inside the fastening parts made of PEEK (polyether ether ketone),  
35  
36 62 the electrical connections to improve plasma ignition, and positioning of the aluminum oxide sample  
37  
38 63 injection capillary. The hyphenation of this new ICP-MS torch with a laser ablation system and the  
39  
40 64 evaluation of its analytical potential in elemental bioimaging is described in this paper.  
41  
42  
43  
44

## 45 **Instrumentation**

### 46 47 48 **Low-flow ICP-MS**

49  
50  
51 67 An Agilent 7500ce ICP-MS (Agilent Technologies, Santa Clara, CA, US) was used to detect the ablated  
52  
53 68 material from the laser ablation system. The conventionally used ICP-Torch was replaced by a quartz  
54  
55 69 torch and a PEEK fastening that were both in-house designed and manufactured to maintain a plasma  
56  
57 70 with only little argon consumption (see Fig. 1). The fastening device was developed to position the torch  
58  
59  
60

1  
2  
3 71 precisely within the ICP's load coil, but it also contains gas tubing, gas connectors, an electrical contact  
4  
5 72 for the plasma ignition spark, as well as the electrical grounding contact for the grounded Pt shield for  
6  
7  
8 73 capacitive decoupling of the torch and the ICP. Cooling of the bubble-shaped quartz torch was achieved  
9  
10 74 by use of compressed air. The sampling interface with an in-house manufactured sampler cone made of  
11  
12 75 brass<sup>22</sup> and a commercially available nickel skimmer cone were used for ion sampling from the low-flow  
13  
14 76 plasma. The sampler cone's orifice was 0.7 mm in diameter, while the skimmer cone's orifice had a  
15  
16 77 diameter of 0.6 mm. Otherwise, the ICP-MS instrument was used as purchased. The pressure in the  
17  
18 78 interface was slightly lower compared to conventional ICP-MS ( $1.69 \times 10^2$  Pa (low flow),  $3.2 \times 10^2$  Pa (high  
19  
20 79 flow)).  
21  
22  
23

24  
25 80 The quartz torch was moved as close as possible to the sampler tip. The latter was introduced into the  
26  
27 81 orifice of the quartz torch to collect the analyte ions generated in the plasma. Only a small gap (ca.  
28  
29 82 0.2 mm) between the sampler base and the quartz torch was left. This gap ensured best sensitivity  
30  
31 83 without allowing cooling air to enter the plasma zone, to avoid disturbing or even extinguishing of the  
32  
33 84 plasma.<sup>21</sup>  
34  
35  
36

37 85 The sample aerosol from the laser ablation system (see below) was introduced through an injector  
38  
39 86 capillary (i.d. 1.0 mm) made of aluminum oxide. Positioning of the capillary and its precise direction to  
40  
41 87 the central channel of the toroidal plasma was crucial to achieve best sensitivities. The position of this  
42  
43 88 capillary had to be optimized prior to any series of analyses and could be fixed mechanically to keep  
44  
45 89 reproducible conditions for all further measurements. The end of the injector capillary was positioned at  
46  
47 90 the beginning of the torch bulb, which was completely filled by the plasma. The distance to the spherical  
48  
49 91 plasma was kept as short as possible and was typically in the range between 1-2 mm.  
50  
51  
52

53  
54 92 Argon gas enters the torch through two concentrically oriented tubes: While the first is the injector  
55  
56 93 capillary for the sample carrier gas flow, the second is the larger tube for the plasma gas flow around the  
57  
58 94 injector tube (see Fig. 1). The plasma gas flow rate was set to the fixed value 0.42 L/min. Directly  
59  
60

1  
2  
3 95 controlled by the ICP-MS instrument, the sample carrier gas flow was guided through the ablation cell  
4  
5 96 and was varied between 0.55 L/min and 1.00 L/min. Compromise conditions were set to the best match  
6  
7  
8 97 of high sensitivity and short washout times of the ablation cell. No further gases were used to maintain  
9  
10 98 the plasma. Torch cooling was achieved by a stream of compressed air that was guided along the outer  
11  
12 99 walls of the quartz torch. The pressure was set to 500 kPa (approximately 70 L/min) to prevent the torch  
13  
14 100 walls from melting. The RF power was varied between 500 W and 1100 W. Extraction lenses and  
15  
16 101 quadrupole parameters were tuned for best sensitivity.  
17  
18  
19

20 102 For optimization of the ICP-MS for the analysis of gelatin standards, the mass trace  $m/z$  127 (iodine) was  
21  
22 103 detected in the transient measurement mode of the instrument with a dwell time set to 0.1 s. During  
23  
24 104 imaging experiments of tissue sections, the dwell time was set to 0.5 s for iodine measurements at  
25  
26 105  $m/z$  127. In case of hematoxylin and eosin (H&E) stained sections, dwell times of 0.4 s ( $^{27}\text{Al}$ ), 0.3 s ( $^{79}\text{Br}$ )  
27  
28 106 and 0.3 s ( $^{81}\text{Br}$ ) were used, respectively. Data evaluation was performed using the data evaluation  
29  
30  
31 107 software ImageJ 1.48f (National Institutes of Health, Bethesda, MD, USA).  
32  
33  
34  
35  
36  
37  
38  
39  
40  
41  
42  
43  
44  
45  
46  
47  
48  
49  
50  
51  
52  
53  
54  
55  
56  
57  
58  
59  
60

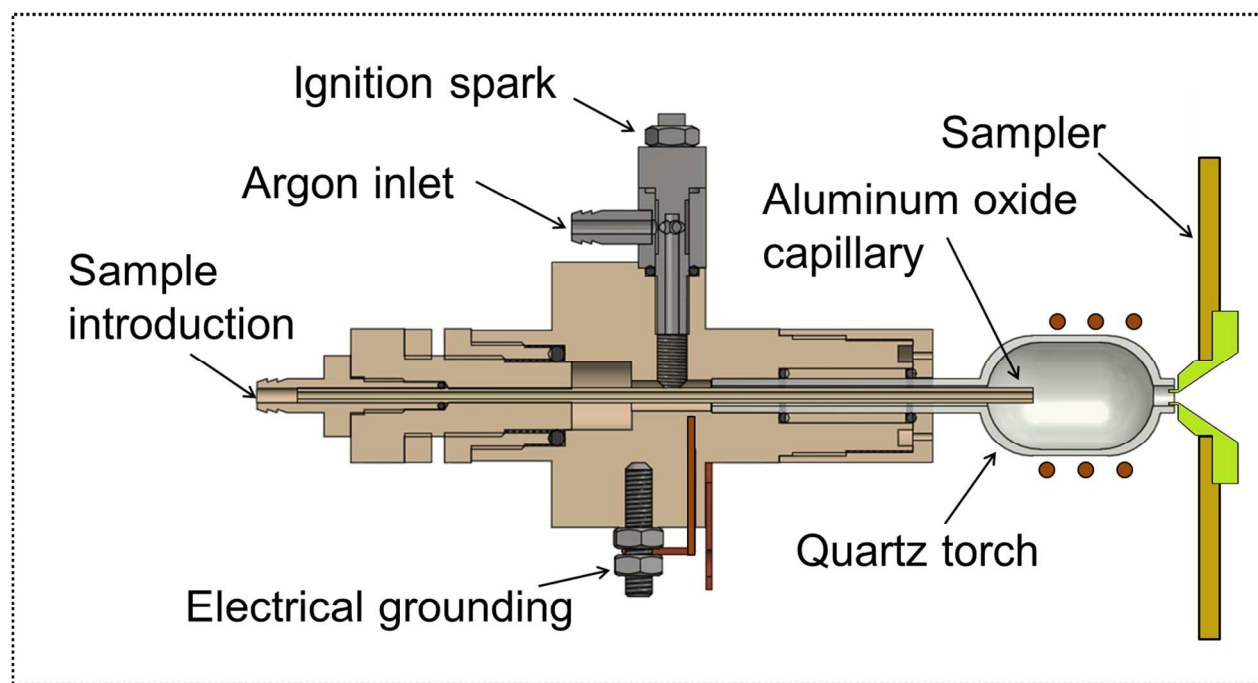
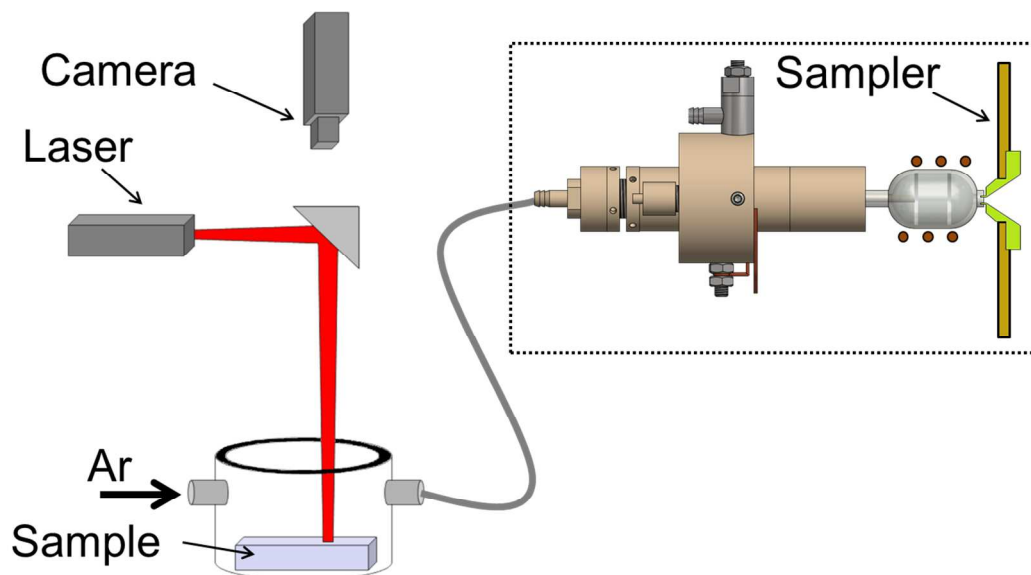


Fig. 1: Schematic setup of the LA-low-flow ICP-MS system (top) and detailed cross section of low-flow torch and fastening (bottom).

Laser ablation

1  
2  
3 113 A commercially available laser ablation system (LSX 213, CETAC Technologies, Omaha, NE, USA) with a  
4  
5 114 frequency quintupled Nd:YAG laser at 213 nm was used. The LA system was equipped with a  
6  
7 115 conventional cyclonic ablation cell with turbulent flow (50 mm (height) x 52 mm (i.d.)). The gelatin  
8  
9 116 standards for optimization of the ICP-MS parameters were ablated in scanning mode with 100  $\mu\text{m}$  spot  
10  
11 117 size, 10  $\mu\text{m}$  space between lines and 100  $\mu\text{m}/\text{s}$  scan speed. The analyzed tissue sections were ablated in  
12  
13 118 a line by line scan with 100  $\mu\text{m}$  spot size. No space between the lines was left and a scan speed of  
14  
15 119 100  $\mu\text{m}/\text{s}$  was applied. The laser parameters fluence and shot frequency were optimized to ensure a  
16  
17 120 homogeneous ablation and sharp edged crater shapes. The laser shot frequency was varied between 10  
18  
19 121 and 20 Hz. Higher frequencies could not be applied with the given setup. The laser energy was varied  
20  
21 122 between 4.9  $\text{J}/\text{cm}^2$  and 7.8  $\text{J}/\text{cm}^2$ . The parameters were set to 7.2  $\text{J}/\text{cm}^2$ , where an optimum signal to  
22  
23 123 noise ratio is observed, and 20 Hz, respectively. To achieve fast wash out, the ablation cell was directly  
24  
25 124 coupled to the low-flow ICP-MS by a transfer line with minimal distance. To achieve highest plasma  
26  
27 125 stability, no further gases such as helium were used to transport the ablated material. Since some  
28  
29 126 authors claimed that the exclusive use of argon shows advantageous wash-out behavior, the usage is  
30  
31 127 well-known for biological samples.<sup>23, 24</sup>

## 32 **Sample preparation**

### 33 Gelatin sections

34  
35 130 For optimization of gas flow and RF power, sections of gelatin standards containing a defined  
36  
37 131 concentration of iodine (270  $\mu\text{g}/\text{mL}$ ) were prepared. Therefore, 100 mg of gelatin were added to 900  $\mu\text{L}$   
38  
39 132 of an aqueous solution of 300  $\mu\text{g}/\text{mL}$  iodine (Ultravist-300, Bayer Vital, Leverkusen, Germany). For  
40  
41 133 homogenization, the solution was heated to 325 K (52  $^{\circ}\text{C}$ ). Gelatin section samples of 12  $\mu\text{m}$  thickness  
42  
43 134 were prepared with a cryomicrotome at 253 K (-20  $^{\circ}\text{C}$ ).

### 44 Kidney sections



1  
2  
3 136 Animal studies were carried out with approval of the state animal welfare committee (ZH1401) and in  
4  
5 137 compliance with the German animal welfare legislation. Male Han-Wistar rats (Charles River, Sulzfeld,  
6  
7 138 Germany) were intravenously dosed with the contrast agent iodixanol (Visipaque 320, GE Healthcare,  
8  
9 139 Buchler GmbH & Co KG, Braunschweig, Germany) with a concentration of 4 g iodine/kg bodyweight. The  
10  
11 140 animals were sacrificed after 24 hours, the left kidneys were removed and cryosections of 12  $\mu\text{m}$   
12  
13 141 thickness were prepared. Tissue sections were stored at 255 K (-18 °C) until usage. Additionally, further  
14  
15 142 kidney sections were stained by means of hematoxylin and eosin (H&E).  
16  
17  
18  
19  
20 143  
21  
22

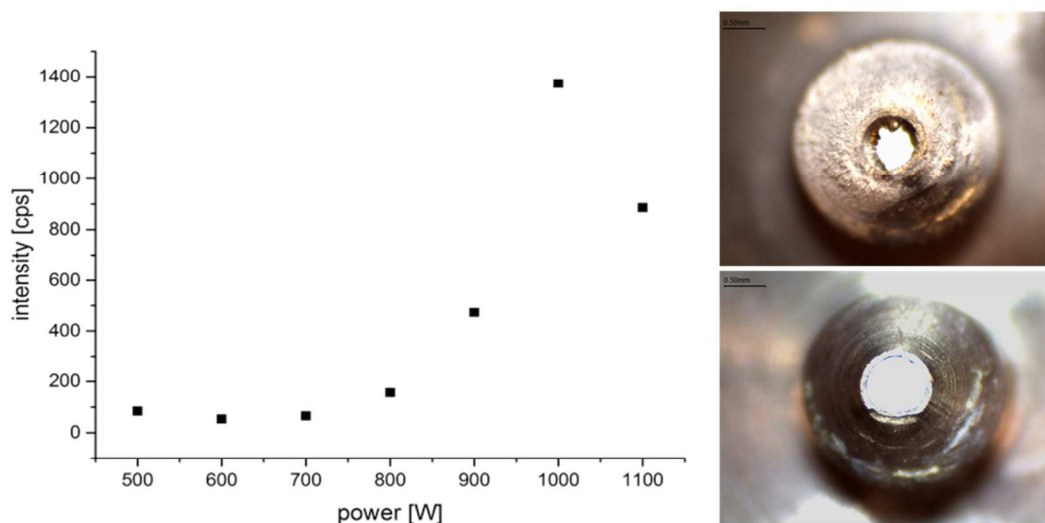
## 23 144 **Results and discussion**

### 26 145 **Optimization of RF power and gas flow rates**

27  
28  
29 146 Optimization was performed by ablating iodine containing gelatin standards (270  $\mu\text{g}/\text{mL}$ ) and averaging  
30  
31 147 the obtained ICP-MS signals at  $m/z$  127 over 100 dwell time periods. All relative standard deviation  
32  
33 148 values were below 2%. The most important parameters for the low-flow ICP-MS were RF power and  
34  
35 149 sample carrier gas flow rate.  
36  
37  
38

39 150 The RF power was optimized in a range between 500 – 1100 W (see Fig. 2). It was found that higher  
40  
41 151 forward powers resulted in higher intensities. However, above 900 W, ablation of quartz from the inner  
42  
43 152 torch wall was observed. After short operation times at generator powers above 900 W, the sampler  
44  
45 153 cone and its sampling orifice tend to be coated with redeposited quartz material. This results in signal  
46  
47 154 depression and corresponding intensity drift of the ICP-MS signals. To a limited extent, this drift may be  
48  
49 155 compensated applying an internal standard correction method.<sup>25-28</sup> This correction procedure is only  
50  
51 156 sufficient for short term measurements and not suited for longer lasting imaging purposes.<sup>22</sup> Therefore,  
52  
53 157 all measurements were performed at 900 W RF power. At this power value, no quartz deposition on the  
54  
55 158 sampler was observed even after several hours of LA-ICP-MS imaging time.  
56  
57  
58  
59  
60

159



160

161 **Fig. 2: Optimization of ICP forward power. Right top: Sampler tip after ca. 10 min with plasma RF**  
162 **power > 1000 W. Right bottom: Sampler tip after 270 min of continuous sample introduction at 900 W**  
163 **RF power.**

164

165 The second optimized parameter was the sample carrier gas flow through the laser ablation cell. This gas  
166 stream transports the sample from the ablation cell into the plasma. It affects not only the plasma  
167 properties significantly, but also the transient peak form generated by the ablated material and  
168 introduced into the plasma. On the one hand, a lower gas flow deteriorates the wash out behavior from  
169 the laser ablation cell and causes broadening of the ICP-MS signals due to longer washout and transport  
170 times from the laser ablation cell into the ICP. Too long washout times reduce the spatial resolution for  
171 imaging purposes. On the other hand, the injector gas velocity directly depending on the sample carrier  
172 gas flow rate has an important influence on the location of highest analyte ion abundance within the  
173 plasma.<sup>29, 30</sup> Since the sampler tip position inside the orifice of the low-flow torch is almost fixed, the  
174 injector gas velocity has to be optimized carefully to precisely adjust the sample ion's location as close to

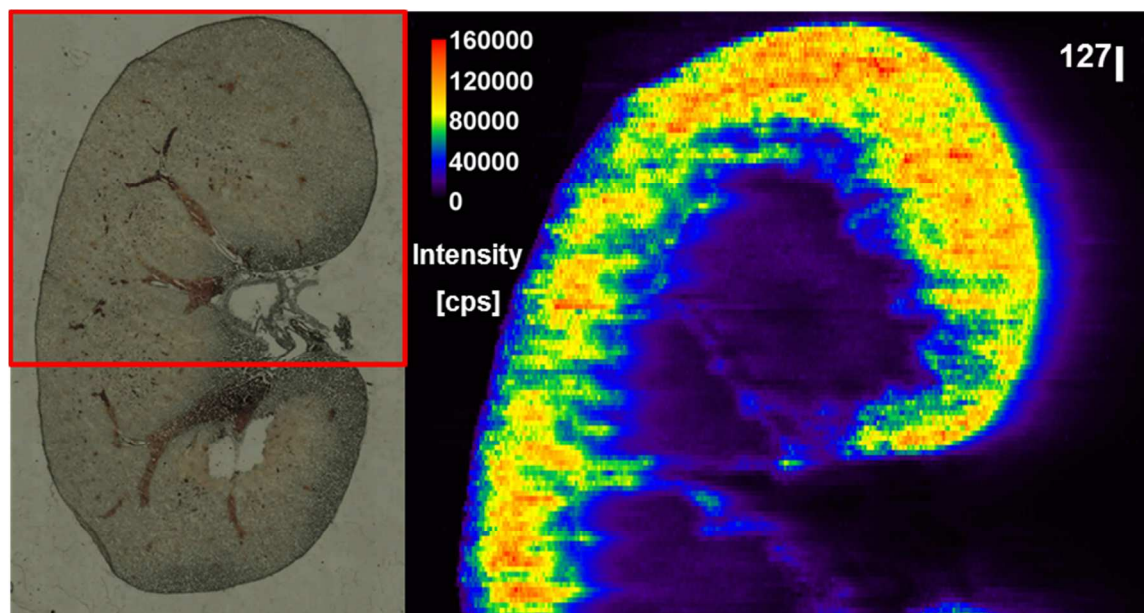
1  
2  
3 175 the sampler orifice as possible. Consequently, the best compromise for the sample carrier gas flow rate  
4  
5 176 in view of sensitivity and spatial resolution of the imaging system had to be found.  
6  
7

8  
9 177 Typical gas flow rates for the laser ablation cell in combination with a commercial ICP-MS system were  
10  
11 178 700 mL/min He and 400 mL/min Ar.<sup>31</sup> No helium was used in the measurements presented here.  
12  
13 179 Accordingly, the sample carrier gas flow rate was varied between 550 mL/min and 1000 mL/min. The  
14  
15 180 best sensitivity was achieved at 650 mL/min Ar gas flow, but at the cost of too long washout times. The  
16  
17 181 highest gas flow rate at 1000 mL/min results in poor sensitivity of the ICP-MS. The best compromise  
18  
19 182 between signal intensity and spatial resolution turned out to be a sample carrier gas flow rate of  
20  
21 183 850 mL/min. Summing up injector and plasma gas flows, the total Ar gas flow into the plasma was only  
22  
23 184 1.27 L/min. These gas flows were adjusted for all measurements. The generator power was set to  
24  
25 185 900 Watt for all imaging measurements.  
26  
27  
28  
29

### 30 186 **Bioimaging of kidney sections**

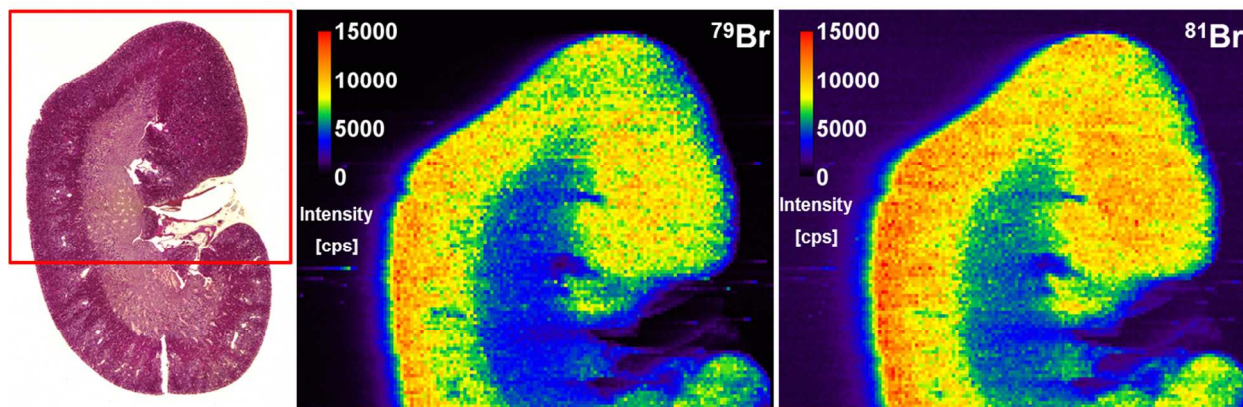
31  
32

33 187 To visualize the distribution of the contrast agent iodixanol in rat kidney, cryosections were analyzed  
34  
35 188 with a spot size of 100  $\mu\text{m}$ . For this purpose, the isotope <sup>127</sup>I was detected using the optimized low-flow  
36  
37 189 ICP-MS system (see Fig. 3). The elemental image shows an inhomogeneous distribution of iodine in the  
38  
39 190 kidney. During the analyses, no signal drift was observed. As expected, highest concentrations of iodine  
40  
41 191 with intensities of up to 160000 counts per second were detected in the cortex. These results correlate  
42  
43 192 to previously published data by computer tomographical (CT) imaging.<sup>32</sup> Investigations with a  
44  
45 193 conventional high flow LA-ICP-MS setup by Reifschneider showed good correlation with the results in the  
46  
47 194 present study.<sup>33</sup> Lower concentrations of the contrast agent were detected in medulla and pelvis of the  
48  
49 195 kidney.  
50  
51  
52  
53  
54  
55  
56  
57  
58  
59  
60



196  
197 **Fig. 3: Microscopic image of a rat kidney tissue slice after delivery of the contrast agent iodixanol (left**  
198 **image). The ablated area is marked with a red box (left). The iodine distribution is presented in the**  
199 **right image as detected with the LA-low-flow ICP-MS system at  $m/z$  127.**

200 Next to the investigation of the iodinated contrast agent iodixanol in the kidney cryosection, a parallel  
201 section of the same kidney was used for hematoxylin and eosin staining. These stains contain bromine  
202 (eosine) and aluminum (hematoxylin) and are therefore accessible to bioimaging by means of ICP-MS.<sup>31</sup>  
203 The kidney section was analyzed for the distribution of  $^{27}\text{Al}$ ,  $^{79}\text{Br}$  and  $^{81}\text{Br}$  (see Fig. 4 for the bromine  
204 isotopes). While aluminum turned out to be homogeneously distributed over the whole kidney (data not  
205 shown), the highest concentration of bromine was detected in the cortex of the kidney and lower  
206 concentrations in the medulla and the pelvis. This was confirmed by the analysis of both bromine  
207 isotopes, which expectedly show the same distribution.



208  
209 **Fig. 4:** Left: Microscopic image; the ablated area is marked with a red box (left). The bromine  
210 distribution image of a kidney cryosection was detected by LA-low-flow ICP-MS at  $m/z$  79 (middle) and  
211  $m/z$  81 (right).

212  
213 **Conclusion**

214 The first low-flow laser ablation ICP-MS system for elemental bioimaging was developed within this  
215 work. After initial optimization of RF power and sample carrier gas flow rates, elemental images of  
216 biological tissues containing iodine, aluminum and bromine as target elements were recorded to prove  
217 the performance and the robustness of the approach.

218 An RF power value of 900 W was found to be best suited for imaging purposes. The sample carrier gas  
219 flow rate was also optimized and the best compromise between signal intensity and spatial resolution  
220 was found to be 0.85 L/min. The second gas flow of the new low-flow ICP torch, namely the plasma gas  
221 flow, was 0.42 L/min and could not be changed. Hence, the total Ar consumption of the presented  
222 system could be reduced significantly to 1.27 L/min.

223 Future developments will be focused on the use of improved ablation cells. Laminar flow profiles in  
224 newly designed cells shall allow shorter wash-out times of the ablated sample aerosol. Consequently, the



1  
2  
3 225 sample carrier gas flow rate can be reduced without losing spatial resolution. In turn, the reduction of  
4  
5 226 the sample carrier gas flow rate would increase the ion sampling efficiency and result in higher signal  
6  
7  
8 227 intensities of the ICP-MS system and thus lower limits of detection. Additionally, the lack of experience  
9  
10 228 regarding the introduction of helium into the low-flow torch was a reason to start the present study first  
11  
12 229 with argon as cell gas. Further experiments with He/Ar gas mixtures are planned for future work.  
13  
14  
15  
16 230  
17  
18  
19 231  
20  
21

22 232 **Acknowledgement**  
23  
24  
25 233 The excellent technical support of the mechanical workshop and glassblowers at the Institute of  
26  
27 234 Inorganic and Analytical Chemistry, University of Münster, is gratefully acknowledged. Parts of this study  
28  
29 235 were supported by the Cells in Motion Cluster of Excellence (CiM-EXC 1003), Münster, Germany (project  
30  
31 236 FF-2013-17).  
32  
33  
34  
35 237  
36  
37

38 238 **References**  
39  
40  
41 239 1. D. Drescher, C. Giesen, H. Traub, U. Panne, J. Kneipp and N. Jakubowski, *Anal. Chem.*, 2012, **84**,  
42 240 9684-9688.  
43 241 2. J. S. Becker, M. V. Zoriy, C. Pickhardt, N. Palomero-Gallagher and K. Zilles, *Anal. Chem.*, 2005, **77**,  
44 242 3208-3216.  
45 243 3. O. Reifschneider, C. A. Wehe, I. Raj, J. Ehmcke, G. Ciarimboli, M. Sperling and U. Karst,  
46 244 *Metallomics*, 2013, **5**, 1440-1447.  
47 245 4. D. Hare, C. Austin and P. Doble, *Analyst*, 2012, **137**, 1527.  
48 246 5. I. Konz, B. Fernández, M. Fernández, R. Pereiro and A. Sanz-Medel, *Anal. Bioanal. Chem.*, 2012,  
49 247 **403**, 2113-2125.  
50 248 6. J. S. Becker, A. Matusch and B. Wu, *Anal. Chim. Acta*, 2014, **835**, 1-18.  
51 249 7. D. Pozebon, G. L. Scheffler, V. L. Dressler and M. A. G. Nunes, *J. Anal. At. Spectrom.*, 2014, **29**,  
52 250 2204-2228.  
53 251 8. D. Urgast, J. Beattie and J. Feldmann, *Curr. Opin. Clin. Nutr. Metab. Care*, 2014, **17**, 431-439.  
54 252 9. G. R. Kornblum, W. Van der Waa and L. de Galan, *Anal. Chem.*, 1979, **51**, 2378-2381.  
55 253 10. J. S. Gordon, P. S. C. van der Plas and L. de Galan, *Anal. Chem.*, 1988, **60**, 372-375.  
56 254 11. M. E. Britske, Y. S. Sukach and L. N. Filimonov, *Zh. Prikl. Spektrosk.*, 1976, **25**, 5-11.  
57  
58  
59  
60

- 1  
2  
3 255 12. M. T. C. de Loos-Vollebregt, L. Tiggelman and L. de Galan, *Spectrochim. Acta, Part B*, 1988, **43B**,  
4 256 773-781.  
5 257 13. P. A. M. Ripson, L. B. M. Jansen and L. de Galan, *Anal. Chem.*, 1984, **56**, 2329-2335.  
6 258 14. N. Praphairaksit, D. Wiederin and R. S. Houk, *Spectrochim. Acta, Part B*, 2000, **55B**, 1279-1293.  
7 259 15. P. S. C. van der Plas, A. C. de Waaij and L. de Galan, *Spectrochim. Acta, Part B*, 1985, **40B**, 1457-  
8 260 1466.  
9 261 16. G. Hieftje, *Spectrochim. Acta, Part B*, 1983, **38B**, 1465-1481.  
10 262 17. J. A. Hopwood, *J. Microelectromech. Syst.*, 2000, **9**, 309-313.  
11 263 18. P. S. C. van der Plas and L. de Galan, *Spectrochim. Acta, Part B*, 1984, **39B**, 1161-1169.  
12 264 19. I. Ishii, H. Tan, S.-k. Chan and A. Montaser, *Spectrochim. Acta, Part B*, 1991, **46**, 901-916.  
13 265 20. A. Klostermeier, C. Engelhard, S. Evers, M. Sperling and W. Buscher, *J. Anal. At. Spectrom.*, 2005,  
14 266 **20**, 308-314.  
15 267 21. A. Scheffer, R. Brandt, C. Engelhard, S. Evers, N. Jakubowski and W. Buscher, *J. Anal. At.*  
16 268 *Spectrom.*, 2006, **21**, 197-200.  
17 269 22. T. Pfeifer, R. Janzen, T. Steingrobe, M. Sperling, B. Franze, C. Engelhard and W. Buscher,  
18 270 *Spectrochim. Acta, Part B*, 2012, **76**, 48-55.  
19 271 23. D. Hare, B. Reedy, R. Grimm, S. Wilkins, I. Volitakis, J. L. George, R. A. Cherny, A. I. Bush, D. I.  
20 272 Finkelstein and P. Doble, *Metallomics*, 2009, **1**, 53-58.  
21 273 24. D. J. Hare, J. K. Lee, A. D. Beavis, A. van Gramberg, J. George, P. A. Adlard, D. I. Finkelstein and P.  
22 274 A. Doble, *Anal. Chem.*, 2012, **84**, 3990-3997.  
23 275 25. M. Bonta, H. Lohninger, V. Laszlo, B. Hegedus and A. Limbeck, *J. Anal. At. Spectrom.*, 2014, **29**,  
24 276 2159-2167.  
25 277 26. M. Bonta, H. Lohninger, M. Marchetti-Deschmann and A. Limbeck, *Analyst*, 2014, **139**, 1521-  
26 278 1531.  
27 279 27. I. Konz, B. Fernández, M. Fernández, R. Pereiro, H. González, L. Álvarez, M. Coca-Prados and A.  
28 280 Sanz-Medel, *Analytical & Bioanalytical Chemistry*, 2013, **405**, 3091-3096.  
29 281 28. C. Austin, F. Fryer, J. Lear, D. Bishop, D. Hare, T. Rawling, L. Kirkup, A. McDonagh and P. Doble, *J.*  
30 282 *Anal. At. Spectrom.*, 2011, **26**, 1494-1501.  
31 283 29. F. Vanhaecke, R. Dams and C. Vandecasteele, *J. Anal. At. Spectrom.*, 1993, **8**, 433-438.  
32 284 30. G. Horlick, S. H. Tan, M. A. Vaughan and C. A. Rose, *Spectrochim. Acta Part B*, 1985, **40**, 1555-  
33 285 1572.  
34 286 31. O. Reifschneider, C. A. Wehe, K. Diebold, C. Becker, M. Sperling and U. Karst, *J. Anal. At.*  
35 287 *Spectrom.*, 2013, **28**, 989-993.  
36 288 32. D. Lenhard, H. Pietsch, M. Sieber, R. Ernst, P. Lengsfeld, P. Ellinghaus and G. Jost, *Invest. Radiol.*,  
37 289 2012, **47**, 503-510.  
38 290 33. O. Reifschneider, PhD thesis, University of Muenster, 2014.

291

292